A statistical approach for polarized parton distributions

Claude Bourrely, Jacques Soffer, Franco Buccella

EPJ manuscript No.
(will be inserted by the editor)

A statistical approach for polarized parton distributions*

Claude Bourrely[1], Jacques Soffer[1], and Franco Buccella[2]

[1] Centre de Physique Théorique, [a]
CNRS-Luminy Case 907,
13288 Marseille Cedex 9, France.
[2] Dipartimento di Scienze Fisiche, Università di Napoli,
Via Cintia, I-80126, Napoli and INFN, Sezione di Napoli, Italy

Received: date / Revised version: date

Abstract. A global next-to-leading order QCD analysis of unpolarized and polarized deep-inelastic scattering data is performed with parton distributions constructed in a statistical physical picture of the nucleon. The chiral properties of QCD lead to strong relations between quarks and antiquarks distributions and the importance of the Pauli exclusion principle is also emphasized. We obtain a good description, in a broad range of x and Q^2, of all measured structure functions in terms of very few free parameters. We stress the fact that at RHIC-BNL the ratio of the unpolarized cross sections for the production of W^+ and W^- in pp collisions, will directly probe the behavior of the $\bar{d}(x)/\bar{u}(x)$ ratio for $x \geq 0.2$, a definite and important test for the statistical model. Finally, we give specific predictions for various helicity asymmetries for the $W^{\pm}, Z$ production in pp collisions at high energies, which will be measured with forthcoming experiments at RHIC-BNL and are sensitive tests of the statistical model for $\Delta\bar{u}(x)$ and $\Delta\bar{d}(x)$.

PACS. 13.88+e quarks polarization – 13.60.Hb deep-inelastic scattering – 12.40.Ee statistical models

1 Introduction

Deep-inelastic scattering (DIS) of leptons on hadrons has been extensively studied, over the last twenty years or so, both theoretically and experimentally. The principal goals of this physics program were, first to elucidate the internal proton structure, in terms of parton distributions, and more recently to test perturbative Quantum Chromodynamics (QCD), which generalizes the parton model. For the unpolarized structure functions, the advent of the HERA physics program gives us access to a broader kinematic range than fixed targets experiments, in x down to a few 10^{-5} and in Q^2 up to several 10^4GeV^2, which allows testing perturbative QCD to next-to-leading order (NLO). As a result, the unpolarized light quarks (u, d) distributions are fairly well determined. Moreover, the data exhibit a clear evidence for a flavor-asymmetric light sea, *i.e.* $\bar{d} > \bar{u}$, which can be understood in terms of the Pauli exclusion principle, based on the fact that the proton contains two u quarks and only one d quark [1]. Larger uncertainties still persist for the gluon (G) and the heavy quarks (s, c) distributions. From the more restricted amount of data on polarized structure functions, the corresponding polarized gluon and s quark distributions $(\Delta G, \Delta s)$ are badly constrained and we just begin to uncover a flavor asymmetry, for the corresponding polarized light sea, namely $\Delta\bar{u} \neq \Delta\bar{d}$. Whereas the signs of the polarized light quarks distributions are essentially well established, $\Delta u > 0$ and $\Delta d < 0$, this is not the case for $\Delta\bar{u}$ and $\Delta\bar{d}$. The objective of this paper is to construct a complete set of polarized parton (all flavor quarks, antiquarks and gluon) distributions and, in particular, we will try to clarify this last point on the polarized light sea.

The polarized parton distributions (PPD) of the nucleon have been extensively studied in the last few years [2,3] and in most models, the PPD are constructed from a set of unpolarized parton distributions, previously determined, from unpolarized DIS data. For example for each quark flavor $q_i(x)$, the corresponding $\Delta q_i(x)$ is taken (at the input energy scale) such that

$$\Delta q_i(x) = a_i(x) \cdot q_i(x) \ , \tag{1}$$

where $a_i(x)$ is a simple polynomial which has to be determined from the polarized DIS data. A similar procedure is used for antiquarks and gluons. As a result, the full determination of all unpolarized and polarized parton distributions involves a large number of free parameters, say around 20-25, which obviously shows a lack of simplicity. In addition, most of these models do not provide a flavor separation [4]for the antiquarks $\bar{q}_i(x)$ and consequently for $\Delta\bar{q}_i(x)$. However, there are recent attempts to make this flavor separation, either using semi-inclusive polarized DIS data [5] or by means of a flavor-symmetry breaking [6]. Our motivation for this work is to use the statistical approach to build up : q_i, Δq_i, $\bar{q}_i$, $\Delta\bar{q}_i$, G and

* Preprint CPT-2001/P.4205, UNIV. NAPLES DSF 29/2001, hep-ph/0109160

[a] Unité Propre de Recherche 7061

ΔG, by means of a very small number of free parameters. A flavor separation for the unpolarized and polarized light sea is automatically achieved in a way dictated by our approach.

The paper is organized as follows. In Section 2, we review the main points of our approach and we describe our method to determine the free parameters of the PPD with the set of experimental data we have used. In Section 3, we show the results obtained for the unpolarized DIS structure functions $F_2^{p,d}(x,Q^2)$ and $xF_3^{\nu N}(x,Q^2)$ in a wide kinematic range, compared with the world data. We show the prediction of the ratio of unpolarized W^+ and W^- cross section at RHIC-BNL, which is sensitive to the $\bar{d}(x)/\bar{u}(x)$ ratio, a challenging question for the statistical approach. Section 4 is devoted to the polarized DIS structure functions $g_1^{p,d,n}(x,Q^2)$. In Section 5, we give our predictions for single and double helicity asymmetries for the heavy gauge boson production ($W^{\pm}, Z$) in pp collisions at high energies, which are sensitive to $\Delta\bar{u}$ and $\Delta\bar{d}$ and will be tested with forthcoming experiments at RHIC-BNL. We give our concluding remarks in Section 6.

2 Basic procedure for the construction of the PPD in the statistical approach

In the statistical approach the nucleon is viewed as a gas of massless partons (quarks, antiquarks, gluons) in equilibrium at a given temperature in a finite size volume. Like in our earlier works on the subject [7–9], we propose to use a simple description of the parton distributions $p(x)$, at an input energy scale Q_0^2, proportional to

$$[\exp[(x-X_{0p})/\bar{x}] \pm 1]^{-1} \ , \tag{2}$$

the *plus* sign for quarks and antiquarks, corresponds to a Fermi-Dirac distribution and the *minus* sign for gluons, corresponds to a Bose-Einstein distribution. Here X_{0p} is a constant which plays the role of the *thermodynamical potential* of the parton p and $\bar{x}$ is the *universal temperature*, which is the same for all partons. Since quarks carry a spin-1/2, it is natural to consider that the basic distributions are $q_i^{\pm}(x)$, corresponding to a quark of flavor i and helicity parallel or antiparallel to the nucleon helicity. This is the way we will proceed. Clearly one has $q_i = q_i^+ + q_i^-$ and $\Delta q_i = q_i^+ - q_i^-$ and similarly for antiquarks and gluons.

We want to recall that the statistical model of the nucleon has been extensively studied in early and more recent papers in the literature [10,11], but in these works at variance with our approach, the statistical picture is first considered in the nucleon rest frame, which is then boosted to the infinite-momentum frame.

From the chiral structure of QCD, we have two important properties which allow to relate quark and antiquark distributions and to restrict the gluon distribution [9,11]:

- The potential of a quark q_i^h of helicity h is opposite to the potential of the corresponding antiquark $\bar{q}_i^{-h}$ of helicity -h

$$X_{0q}^h = -X_{0\bar{q}}^{-h} \ . \tag{3}$$

- The potential of the gluon G is zero

$$X_{0G} = 0 \ . \tag{4}$$

From well established features of the u and d quark distributions extracted from DIS data, we anticipate some simple relations between the potentials:

- $u(x)$ dominates over $d(x)$, therefore one can expect $X_{0u}^+ + X_{0u}^- > X_{0d}^+ + X_{0d}^-$
- $\Delta u(x) > 0$, therefore $X_{0u}^+ > X_{0u}^-$
- $\Delta d(x) < 0$, therefore $X_{0d}^- > X_{0d}^+$.

So we expect X_{0u}^+ to be the largest thermodynamical potential and X_{0d}^+ the smallest one. In fact, as we will see from the discussion below, we have the following ordering

$$X_{0u}^+ > X_{0d}^- \sim X_{0u}^- > X_{0d}^+ \ . \tag{5}$$

Eq. (5) is consistent with the previous determinations of the potentials [7], including the one with dimensional values in the rest system [11]. By using Eq. (3), this ordering leads immediately to some important consequences for antiquarks, namely

i) $\bar{d}(x) > \bar{u}(x)$, the flavor symmetry breaking which also follows from the Pauli exclusion principle, as recalled above. This was already confirmed by the violation of the Gottfried sum rule [12,13].

ii) $\Delta\bar{u}(x) > 0$ and $\Delta\bar{d}(x) < 0$, which remain to be checked and this will be done in hadronic collisions at RHIC-BNL (see Section 6).

Note that since $\bar{u}^+(x) \sim \bar{d}^+(x)$, we have

$$\Delta\bar{u}(x) - \Delta\bar{d}(x) \sim \bar{d}(x) - \bar{u}(x) \ , \tag{6}$$

so the flavor symmetry breaking is almost the same for unpolarized and polarized distributions.

Let us now come back to the ordering in Eq. (5) to justify it. We consider the isovector contributions to the structure functions g_1 and F_2, which are the differences on proton and neutron targets. In the QCD parton model they read

$$2xg_1^{(p-n)}(x,Q^2) = \frac{1}{3}x[(\Delta u + \Delta\bar{u})(x,Q^2) - (\Delta d + \Delta\bar{d})(x,Q^2)] \otimes \Delta C_{NS}(x,Q^2) \ , \tag{7}$$

and

$$F_2^{(p-n)}(x,Q^2) = \frac{1}{3}x[(u+\bar{u})(x,Q^2)) - (d+\bar{d})(x,Q^2))] \otimes C_{NS}(x,Q^2) \ , \tag{8}$$

where $\Delta C_{NS}(x,Q^2)$ and $C_{NS}(x,Q^2)$ denote the spin-dependent and spin-independent perturbative QCD coefficients [2]. Since they differ only in a non-negligible way for very small

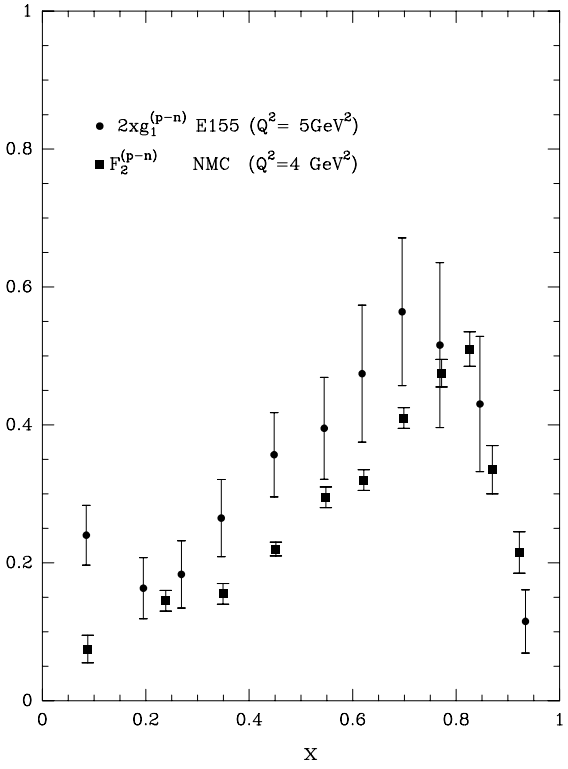

Fig. 1. The isovector structure functions $2xg_1^{(p-n)}(x)$ and $F_2^{(p-n)}(x)$. Data is taken from Refs. [13,15].

x, say $x \leq 0.05$, we see that $2xg_1^{(p-n)} - F_2^{(p-n)}$ is only sensitive to the helicity *minus* components of the u and d quark distributions, so we get

$$[2xg_1^{(p-n)} - F_2^{(p-n)}](x,Q^2) \sim$$
$$-\frac{2}{3}[(u^- - d^-)(x,Q^2)) - (\bar{u}^- - \bar{d}^-)(x,Q^2))] \otimes C_{NS}(x,Q^2) \quad (9)$$

At this stage it is instructive to look at the available data shown in Fig. 1. We notice that these two functions have very similar shapes and their difference is small and mainly positive, except perhaps for large x. In order to try to identify the origin of this experimental fact, let us look at the integrals of these functions divided by x. The first one is twice the Bjorken sum rule [14], for which the best world estimate is $I_{Bj} = 0.176 \pm 0.005 \pm 0.007$ [15] and the second one is the Gottfried sum rule [12] whose value is $I_G = 0.235 \pm 0.026$ [13]. As a result using Eq. (9) one obtains, say for $Q^2 = 5\text{GeV}^2$,

$$\int_0^1 dx[(d^-(x) - u^-(x)) + (\bar{d}^-(x) - \bar{u}^-(x))]$$
$$= 0.175 \pm 0.06\ . \quad (10)$$

Now from the NMC result on the Gottfried sum rule one has

$$\int_0^1 dx[\bar{d}(x) - \bar{u}(x)] = 0.16 \pm 0.03\ . \quad (11)$$

By comparing these two results we can assume, to a good approximation, the following relation for the helicity *minus* distributions

$$d^-(x) = u^-(x)\ . \quad (12)$$

It follows from our procedure to construct antiquark distributions from quark distributions described above (see Eq. (3)), that we have automatically for the helicity *plus* antiquark distributions

$$\bar{d}^+(x) = \bar{u}^+(x)\ , \quad (13)$$

which makes Eqs. (10) and (11) perfectly compatible. Indeed, as we will see below, Eq. (12) is rather well satisfied in the final determination of the distributions, after fitting the data.

Let us now complete the description of our parametrization. As stated above, the essential ingredient for quarks and antiquarks is a Fermi-Dirac distribution, as shown in Eq. (2), but we expect this piece to die out in the small x region, so we have to multiply it by a factor $AX_{0q}^h x^b$, where $b > 0$. In addition to A, a flavor and helicity independent normalization constant, we have introduced the factor X_{0q}^h which is needed to get a good description of the data. It is not required by the simple Fermi-Dirac expression but, due to the ordering in Eq. (5), it will secure the correlation between the shape of a given distribution and its first moment [7,16]. It is also in agreement with what has been found from data for the second and third moments of the valence partons [17]. The small x region is characterized by a rapid rise as $x \to 0$ of the distribution, which should be dominated by a universal diffractive term, flavor and helicity independent, coming from the Pomeron universality. Therefore we must add a term of the form $\tilde{A}x^{\tilde{b}}/[\exp(x/\bar{x}) + 1]$, where $\tilde{b} < 0$ and $\tilde{A}$ is a normalization constant. So for the light quarks $q = u,\ d$ of helicity $h = \pm$, at the input energy scale $Q_0^2 = 4\text{GeV}^2$, we take

$$xq^h(x,Q_0^2) = \frac{AX_{0q}^h x^b}{\exp[(x - X_{0q}^h)/\bar{x}] + 1} + \frac{\tilde{A}x^{\tilde{b}}}{\exp(x/\bar{x}) + 1}\ , \quad (14)$$

and similarly for the light antiquarks

$$x\bar{q}^h(x,Q_0^2) = \frac{\bar{A}(X_{0q}^{-h})^{-1}x^{2b}}{\exp[(x + X_{0q}^{-h})/\bar{x}] + 1} + \frac{\tilde{A}x^{\tilde{b}}}{\exp(x/\bar{x}) + 1}\ . \quad (15)$$

Here we take $2b$ for the power of x and not b as for quarks, an assumption we will try to justify later. For the strange quarks and antiquarks, s and $\bar{s}$, given our poor knowledge on both unpolarized and polarized distributions, we take the particular choice

$$xs(x,Q_0^2) = x\bar{s}(x,Q_0^2) = \frac{1}{4}[x\bar{u}(x,Q_0^2) + x\bar{d}(x,Q_0^2)]\ , \quad (16)$$

and

$$x\Delta s(x,Q_0^2) = x\Delta\bar{s}(x,Q_0^2) = \frac{1}{3}[x\Delta\bar{d}(x,Q_0^2) - x\Delta\bar{u}(x,Q_0^2)] \ . \tag{17}$$

This particular choice gives rise to a large negative $\Delta s(x,Q_0^2)$ and we will come back to it below, in the discussion of our results (see Section 4). The charm quarks c , both unpolarized and polarized, are set to zero at $Q_0^2 = 4\mathrm{GeV}^2$. Finally concerning the gluon distribution, as indicated above, we use a Bose-Einstein expression given by

$$xG(x,Q_0^2) = \frac{A_G x^{b_G}}{\exp(x/\bar{x}) - 1} \ , \tag{18}$$

with a vanishing potential and the same temperature $\bar{x}$. This choice is consistent with the idea that hadrons, in the DIS regime, are black body cavities for the color fields. It is also reasonable to assume that for very small x, $xG(x,Q_0^2)$ has the same behavior as $x\bar{q}(x,Q_0^2)$, so we will take $b_G = 1+\tilde{b}$. Since the normalization constant A_G is determined from the momentum sum rule, our gluon distribution has no free parameter. For the sake of completeness, we also need to specify the polarized gluon distribution and we take the particular choice

$$x\Delta G(x,Q_0^2) = 0 \ , \tag{19}$$

consistently with Eq. (4). As usual, the valence contributions are defined as $q_{val} = q - \bar{q}$, so A and $\bar{A}$ are determined using the normalization of $u_{val}(x)$ and $d_{val}(x)$, whose first moments are respectively 2 and 1.

To summarize our parametrization involves a total of *eight* free parameters

$$\bar{x} \ , X_{0u}^+ \ , X_{0u}^- \ , X_{0d}^- \ , X_{0d}^+ \ , b \ , \tilde{b} \text{ and } \tilde{A} \ . \tag{20}$$

In order to determine these parameters, we use a fitting procedure on a selection of 233 data points at Q^2 values, as close as possible to our input energy scale $Q_0^2 = 4\mathrm{GeV}^2$ and the χ^2 value we obtain is 322. For unpolarized DIS, we have considered $F_2^p(x,Q^2)$ from NMC, BCDMS, E665 and ZEUS, $F_2^d(x,Q^2)$ from NMC, E665 and $xF_3^{\nu N}(x,Q^2)$ from CCFR [13],[18]-[28]. For polarized DIS we have considered $g_1^{p,d,n}(x,Q^2)$ from SMC, E154 and E155 [15,29,30]. The average χ^2 per point is 1.38, which is not impressive, but one has to keep in mind that we have greatly restricted the number of free parameters by means of our underlying physical picture. To get a better feeling on the distribution of this χ^2, let us give some details on our results. We find a χ^2/pt of 0.5 for the NMC data on F_2^p and F_2^d, whereas it is 1.5 for the ZEUS data on F_2^p and CCFR data on xF_3. For the polarized structure functions, the combined E155 and SMC data for g_1^p lead to $\chi^2/pt = 2.5$, whereas it is only 0.85, for g_1^n with the E154 and SMC combined data. The *five* free parameters, *one* temperature and *four* potentials, which determine the Fermi-Dirac functions at the input energy scale $Q_0^2 = 4\mathrm{GeV}^2$ are

$$\bar{x} = 0.09907,\ X_{0u}^+ = 0.46128,\ X_{0u}^- = 0.29766,$$
$$X_{0d}^- = 0.30174 \text{ and } X_{0d}^+ = 0.22775 \ . \tag{21}$$

From the above discussion which led us to Eqs. (12) and (13), we observe that the fit yields $X_{0u}^- \sim X_{0d}^-$, in agreement with our expectations. We show in Figs. 2, 3 the Fermi-Dirac functions Eq. (2) for light quarks and antiquarks, respectively. They exhibit a flat behavior in the small x region, at variance with the rising trend of the parton distributions, which ought to be described by the universal diffractive term (see Eqs. (14, 15)). It is also interesting to make one more observation from the above values of these potentials. It turns out that if we impose the following simple relations $X_{0d}^- = X_{0u}^-$, $X_{0u}^+ = 3/2X_{0u}^-$ and $X_{0d}^+ = 3/4X_{0u}^-$, we can get an equally good fit of the data with $X_{0u}^- = 0.30549$. This choice reduces the number of free parameters for the potentials from four to one, but we cannot justify it and it might be fortuitous.

For the remaining *three* free parameters b , $\tilde{b}$ and $\tilde{A}$, the fit gives the values

$$b = 0.40962,\ \tilde{b} = -0.25347 \text{ and } \tilde{A} = 0.08318 \ . \tag{22}$$

Finally the parameters A, $\bar{A}$ and A_G determined by normalization conditions and momentum sum rule, have the following values

$$A = 1.74938,\ \bar{A} = 1.90801 \text{ and } A_G = 14.27535 \ . \tag{23}$$

We show in Figs. 4, 5, the different helicity components of the light quarks and antiquarks, respectively, at $Q^2 = 20\mathrm{GeV}^2$, after a NLO evolution. They all have the same rising behavior in the small x-region, which is driven by the universal diffractive term. We note that after NLO evolution, we still have $u^- \sim d^-$ and $\bar{u}^+ \sim \bar{d}^+$. In Fig. 6, we display the x-shapes of the full set of unpolarized parton distributions, where one sees a non zero c quark distribution generated by the Q^2 evolution. Note that $u^- \sim d^-$ implies

$$u(x) - d(x) \sim \Delta u(x) - \Delta d(x) \tag{24}$$

at least up to $Q^2 \sim 20\mathrm{GeV}^2$. This is a specific feature of our quark distributions which is not fulfilled in most parametrizations [3]. In order to compute the evolved distributions, we have used the following method: all parton distributions and splitting functions are decomposed in terms of Chebyshev polynomials, then the DGLAP equations at NLO are solved by a Runge-Kutta method [31] or by a semianalytic method [32]. The renormalization scheme adopted is $\overline{MS}$ with $\Lambda_{\overline{MS}}[n_f = 3] = 300\mathrm{MeV}$ and we also use the $\overline{MS}$ factorization scheme in defining the NLO relation between the parton distributions and the structure functions [1]. We have checked that both methods are consistent, within the numerical accuracy. All the results shown in the figures are calculated at NLO.

Let us now comment on the values obtained for some of these parameters. First, it is interesting to note that

[1] However, we could have chosen another scheme with the same functional forms for the parton distributions, which would have led to slightly different values of the fitted parameters.

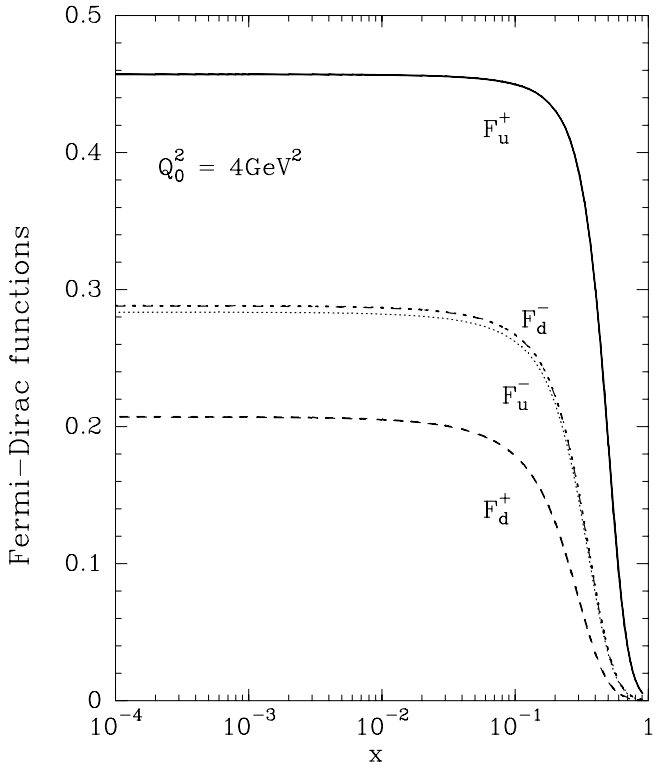

Fig. 2. The Fermi-Dirac functions for quarks $F_q^h = X_{0q}^h/(\exp[(x - X_{0q}^h)/\bar{x}] + 1)$ at the input energy scale $Q_0^2 = 4\text{GeV}^2$, as a function of x.

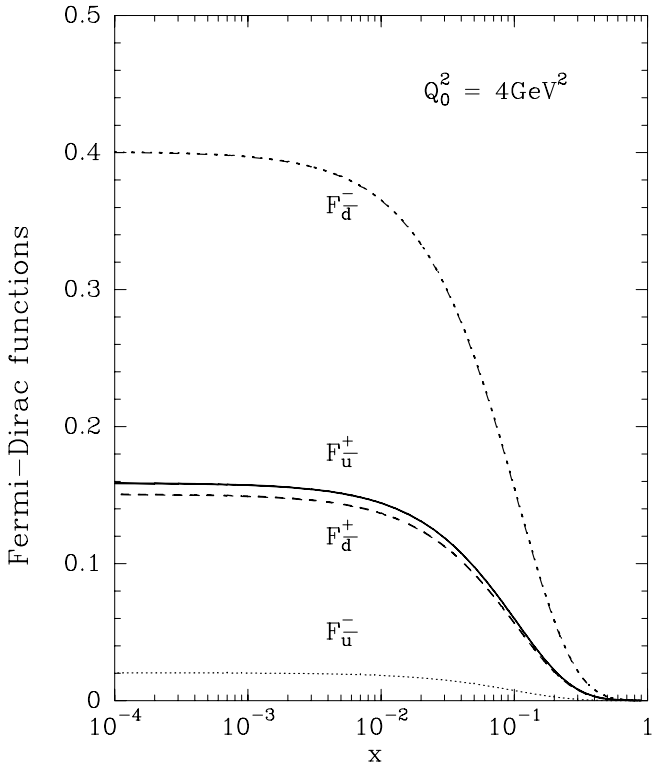

Fig. 3. The Fermi-Dirac functions for antiquarks $F_{\bar{q}}^h = 1/X_{0\bar{q}}^h(\exp[(x + X_{0\bar{q}}^h)/\bar{x}] + 1)$ at the input energy scale $Q_0^2 = 4\text{GeV}^2$, as a function of x.

A and $\bar{A}$, the normalizations of quarks and antiquarks, come close to each other. Next, concerning the power of x for which we took, b for quarks and $2b$ for antiquarks, let us try to understand this fact and the value of b. The universal diffractive term, involving $\tilde{b}$ and $\tilde{A}$, is absent in the physical quantity $x\bar{d}(x) - x\bar{u}(x)$, which was extracted recently in Ref. [33] (see Section 3 for further comments on these data). This quantity rises in the region $0.01 \leq x \leq 0.2$, whereas the antiquark Fermi-Dirac functions decrease (see Fig. 3). This rising behavior is simply obtained if one multiplies these functions by $x^{0.8}$. Another physical quantity which does not contain the universal diffractive term is $xF_3^{\nu N}(x)$, because it involves the difference $q_i(x) - \bar{q}_i(x)$. In the region $0.01 \leq x \leq 0.2$, quarks dominate over antiquarks (see Fig. 6) and we know that $xF_3^{\nu N}(x)$ rises. This behavior is obtained if one multiplies the quark Fermi-Dirac function by $x^{0.4}$, in agreement with Eq. (22).

In the next section we will compare our calculations obtained using these parton distributions, with the existing experimental world data, for the unpolarized DIS structure functions $F_2^{p,d}(x, Q^2)$ and $xF_3^{\nu N}(x, Q^2)$, in a wide kinematic range. We will also show the prediction of the ratio of unpolarized W^+ and W^- cross sections at RHIC-BNL, which is sensitive to the $\bar{d}(x)/\bar{u}(x)$ ratio, a challenging question for the statistical approach.

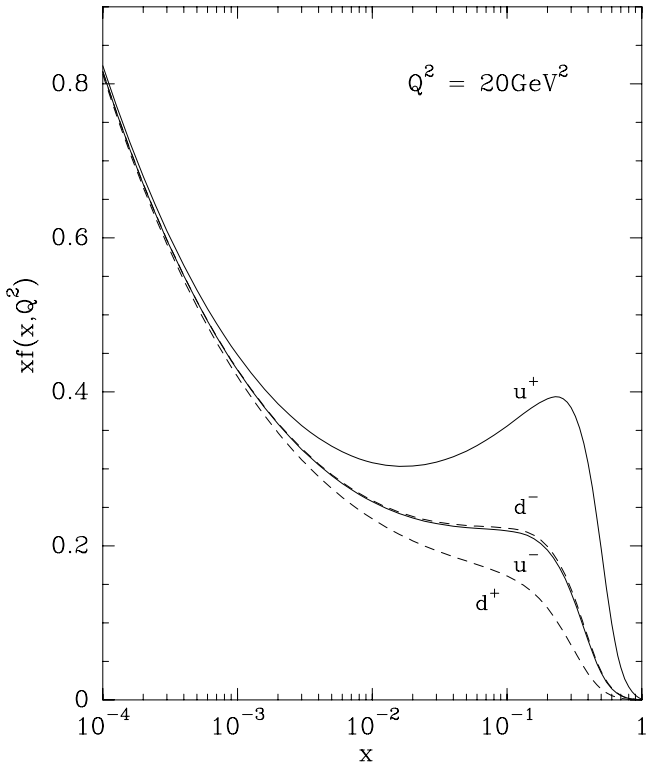

Fig. 4. The different helicity components of the light quark distributions after NLO evolution, at $Q^2 = 20\text{GeV}^2$, as a function of x.

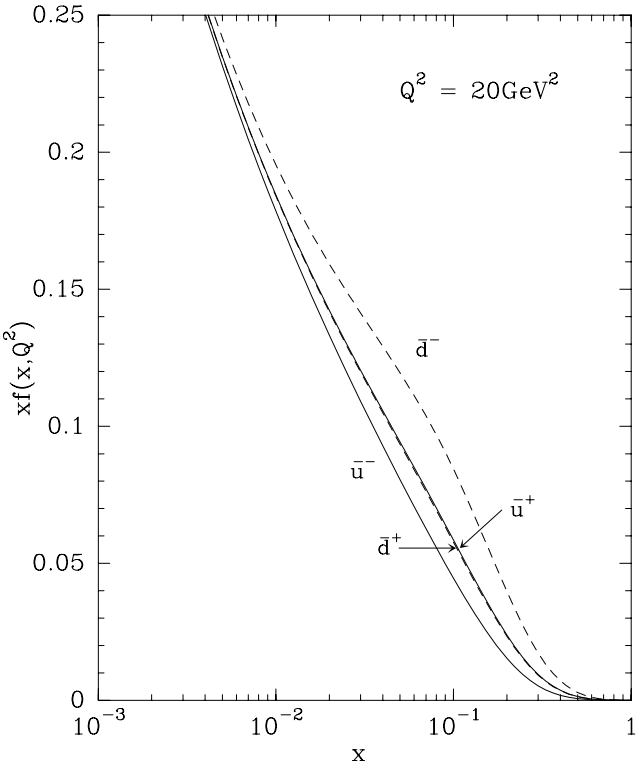

Fig. 5. The different helicity components of the light antiquark distributions after NLO evolution, at $Q^2 = 20\text{GeV}^2$, as a function of x.

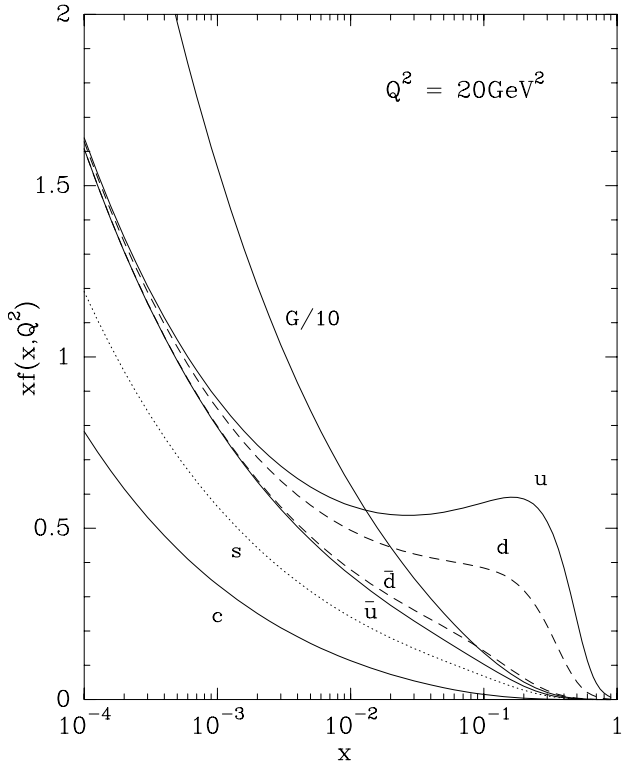

Fig. 6. The different unpolarized parton distributions (f =u, d, $\bar{u}$, $\bar{d}$, s, c and G) after NLO evolution, at $Q^2 = 20\text{GeV}^2$, as a function of x.

3 Experimental tests for unpolarized DIS

We first consider μp and ep DIS for which several experiments have yielded a large number of data points on the structure function $F_2^p(x, Q^2)$. We have compared our calculations with fixed target measurements NMC, BCDMS and E665, which cover a rather limited kinematic region in Q^2 and also with the data at HERA from the H1 and ZEUS Collaborations. These last data cover a very large Q^2 range, up to $Q^2 = 10^4\text{GeV}^2$ or so and probe the very low x region which is dominated by the rising behavior of the universal diffractive term.

The comparison of our results with the data is shown in Figs. 7, 8, 9 and 10. We notice in Fig. 7 that the very low Q^2 range accessible by E665, requires a downwards Q^2 evolution which is achieved successfully down to $Q^2 = 1\text{GeV}^2$ or so, but we fail to reproduce the data much below than that. The H1 and ZEUS data are fairly well described as shown in Figs. 8 and 9, respectively. Finally, we present a compilation of the data, including NMC and BCDMS, in Fig. 10 which is in very good agreement with our theoretical curves. From measurements over a large Q^2 range, it is possible to improve the determination of the gluon density by analyzing the scaling violations. On Fig. 11 we see that $xG(x, Q^2)$ exhibits a fast rising behavior in the low x region, which is fairly consistent with our simple parametrization (see Eq. (18)). Note that, $xG(x, Q^2)$ is predicted to increase with Q^2 as shown in the figure. Next we consider $F_2^d(x, Q^2)$ obtained on a deuterium fixed target from NMC, BCDMS and E665 data. The comparison of these very accurate data with our results is shown on Figs. 12, 13 and 14, respectively. The agreement is also excellent, except for the very low Q^2 region of E665, as for the proton case. Finally the high statistics νN DIS data from CCFR allows to extract the $xF_3^{\nu N}(x, Q^2)$ structure function, which is successfully compared to our results on Fig. 15. The heavy quark corrections are only relevant in the small x region, where unfortunately the experimental errors are large, but we have checked that we get a contribution consistent with the data [28].

To complete our tests of the unpolarized parton distributions, we must come back to the important question of the flavor asymmetry of the light antiquarks. Our determination of $\bar{u}(x, Q^2)$ and $\bar{d}(x, Q^2)$ is perfectly consistent with the violation of the Gottfried sum rule, for which we found $I_G = 0.2493$ for $Q^2 = 4\text{GeV}^2$. Nevertheless there remains an open problem with the x distribution of the ratio $\bar{d}/\bar{u}$ for $x \geq 0.2$. According to the Pauli principle this ratio should be above 1 for any value of x. However, recently the E866/NuSea Collaboration [33] has released the final results corresponding to the analysis of their full data set of Drell-Yan yields from an 800 GeV/c proton beam on hydrogen and deuterium targets and they obtain the ratio $\bar{d}/\bar{u}$ shown in Fig. 16 for $Q^2 = 54\text{GeV}^2$. Although the errors are rather large in the high x region, the statistical approach disagrees with the trend of the data. However in the small x region, where the data are remarkably precise, there is a good agreement with our predictions. Clearly by increasing the number of free parameters, it is possible to build up a scenario which leads to the drop off of this

ratio for $x \geq 0.2$. For example this was achieved in Ref. [37], as shown by the dashed curve in Fig. 16. There is no such freedom in the statistical approach, since quark and antiquark distributions are strongly related. One way to clarify the situation is, either to improve the statistical accuracy on the Drell-Yan yields which seems rather unlikely, or to call for the measurement of another observable sensitive to $\bar{u}(x)$ and $\bar{d}(x)$. One possibility is the ratio of the unpolarized cross sections for the production of W^+ and W^- in $p\bar{p}$ collisions, which will directly probe the behavior of the $\bar{d}(x)/\bar{u}(x)$ ratio. Let us recall that if we denote $R_W(y) = (d\sigma^{W^+}/dy)/(d\sigma^{W^-}/dy)$, where y is the W rapidity, we have [38] at the lowest order

$$R_W(y, M_W^2) = \frac{u(x_a, M_W^2)\bar{d}(x_b, M_W^2) + \bar{d}(x_a, M_W^2)u(x_b, M_W^2)}{d(x_a, M_W^2)\bar{u}(x_b, M_W^2) + \bar{u}(x_a, M_W^2)d(x_b, M_W^2)}, \quad (25)$$

where $x_a = \sqrt{\tau}e^y$, $x_b = \sqrt{\tau}e^{-y}$ and $\tau = M_W^2/s$. This ratio R_W, such that $R_W(y) = R_W(-y)$, is accessible with a good precision at RHIC-BNL [39] and at $\sqrt{s} = 500$GeV for $y = 0$, we have $x_a = x_b = 0.16$. So $R_W(0, M_W^2)$ probes the $\bar{d}(x)/\bar{u}(x)$ ratio at $x = 0.16$. Much above this x value, the accuracy of Ref. [33] becomes poor. In Fig. 17 we compare the results for R_W using two different calculations. In both cases we take the u and d quark distributions obtained from the present analysis, but first we use the $\bar{u}$ and $\bar{d}$ distributions of the statistical approach (solid curve in Fig. 16) and second the $\bar{u}$ and $\bar{d}$ from Ref. [37] (dashed curve in Fig. 16). Notice that the energy scale M_W^2 is much higher than in the E866/NuSea data, so one has to take into account the Q^2 evolution. At $\sqrt{s} = 200$GeV for $y = 0$, we have $x_a = x_b = 0.40$ and, although the $W^\pm$ yield is smaller at this energy, the effect on $R_W(0, M_W^2)$ is strongly enhanced, as seen in Fig. 17. This excellent test, must be done in the near future.

4 Experimental tests for polarized DIS

Since our approach is based on the direct construction of the quark and antiquark distributions of a given helicity $q_i^\pm$ and $\bar{q}_i^\pm$, from the previous results we immediately obtained Δq_i and $\Delta\bar{q}_i$ for each flavor. We display in Fig. 18 these distributions $x\Delta f(x, Q^2)$ versus x, at $Q^2 = 20\text{GeV}^2$, after a NLO evolution. As we mentioned earlier, we took $\Delta G = \Delta c = \Delta\bar{c} = 0$ at the input energy scale, but as shown in the Figure, this is no longer true after the Q^2 evolution. We notice that the distributions are positive for u, $\bar{u}$ and G and negative for d, $\bar{d}$, $s(\bar{s})$ and c, which remain extremely small. We have also checked that our $\Delta q_i(x)$ satisfy the positivity conditions at the leading twist level obtained in Ref. [40]. Recently, the HERMES Collaboration has presented new semi-inclusive data [41] with greater precision, which allows a good flavor separation of the light quarks and these data are shown in Fig. 19. However from this data analysis one cannot achieve a flavor separation for the antiquarks, so $\Delta q_s/q_s$ represents the polarization of sea quarks assuming flavor symmetry, *i.e.*

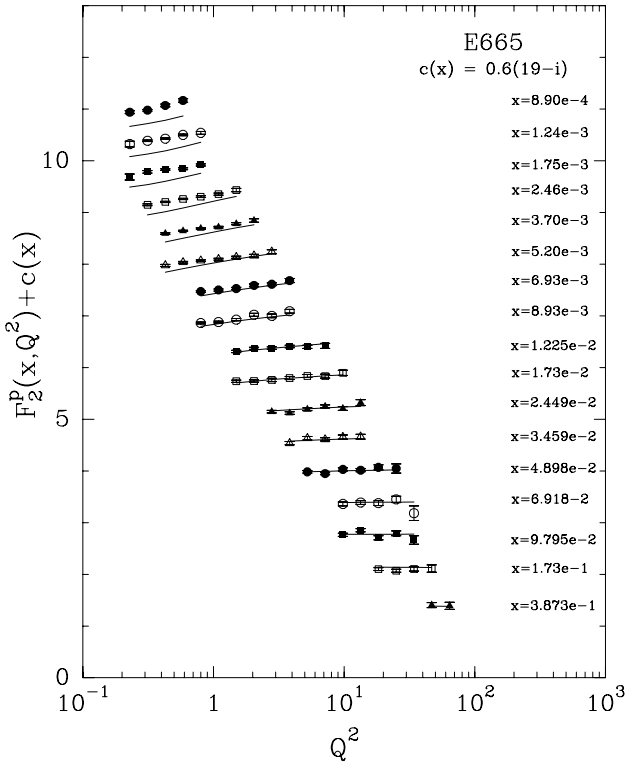

Fig. 7. $F_2^p(x, Q^2)$ as function of Q^2 for fixed x, E665 data [22]. The function $c(x_i) = 0.6(19 - i)$, $i = 1$ corresponds to $x = 8.9\ 10^{-4}$.

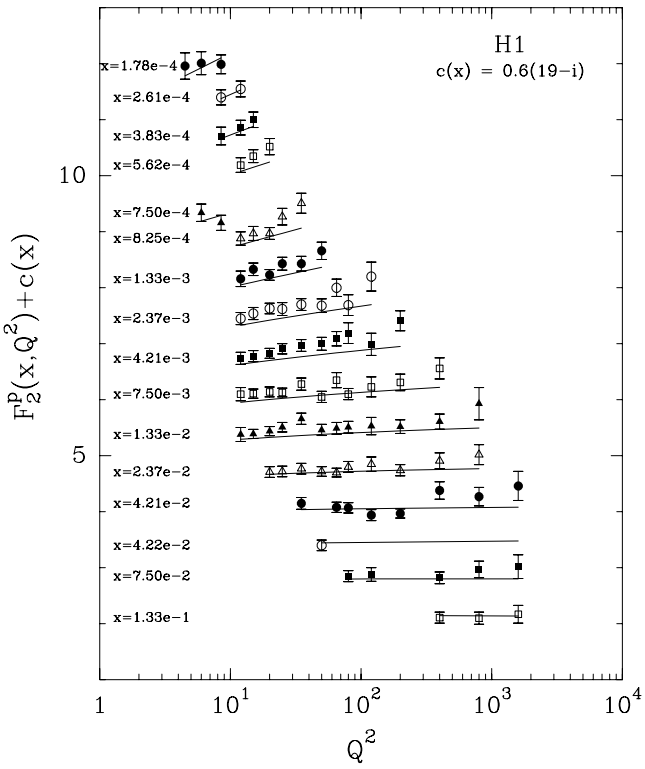

Fig. 8. $F_2^p(x, Q^2)$ as function of Q^2 for fixed x, H1 data [34, 35]. The function $c(x_i) = 0.6(19 - i)$, $i = 1$ corresponds to $x = 1.78\ 10^{-4}$.

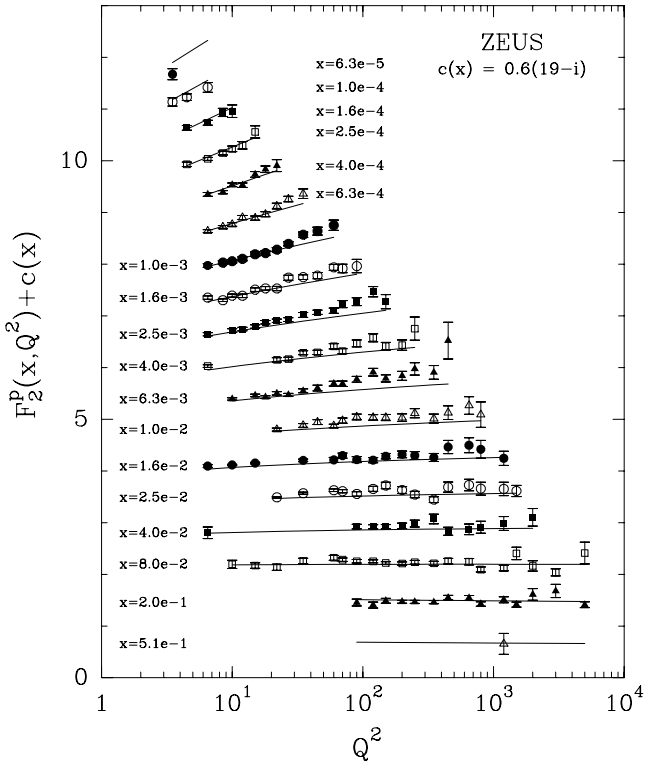

Fig. 9. $F_2^p(x, Q^2)$ as function of Q^2 for fixed x, ZEUS data [25, 26]. The function $c(x_i) = 0.6(19 - i)$, $i = 1$ corresponds to $x = 6.3\ 10^{-5}$.

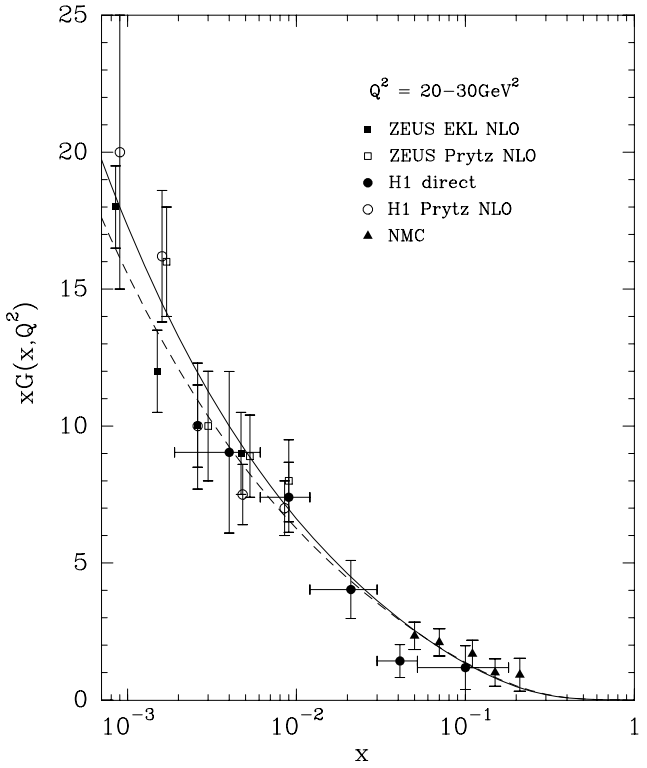

Fig. 11. Comparison of $xG(x, Q^2)$ at $Q^2 = 20 - 30\text{GeV}^2$ (dashed-solid) with experimental determination from NMC [18], H1 [36] and ZEUS [24] experiments.

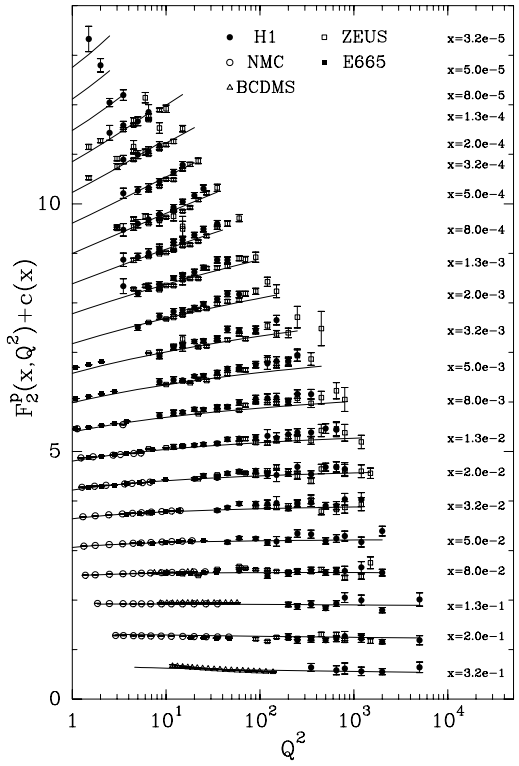

Fig. 10. $F_2^p(x, Q^2)$ as function of Q^2 for fixed x, $c(x) = 0.6(i_x - 0.4)$, $i_x = 1 \to x = 0.32$, rebinned data H1, ZEUS, E665, NMC, BCDMS. (Presentation of data, courtesy of R. Voss).

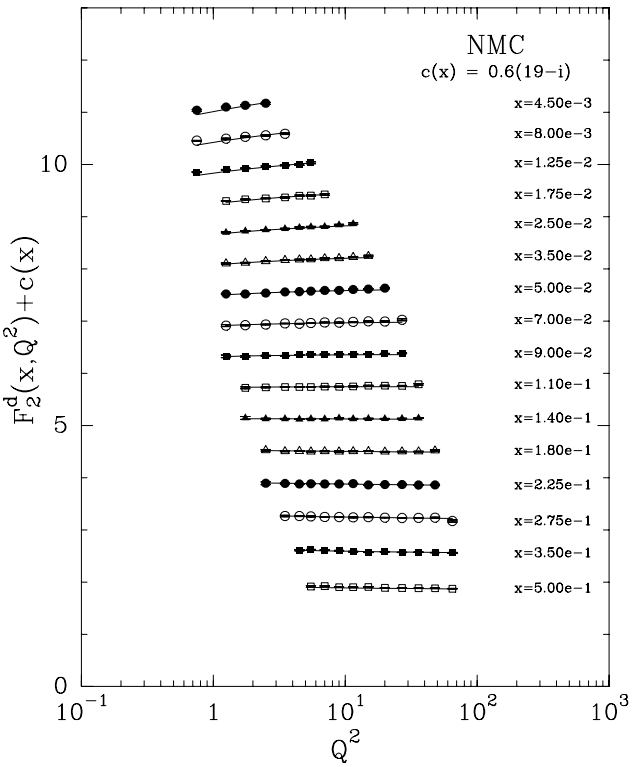

Fig. 12. $F_2^d(x, Q^2)$ as function of Q^2 for fixed x, NMC data [19]. The function $c(x_i) = 0.6(19 - i)$, $i = 1$ corresponds to $x = 4.5\ 10^{-3}$.

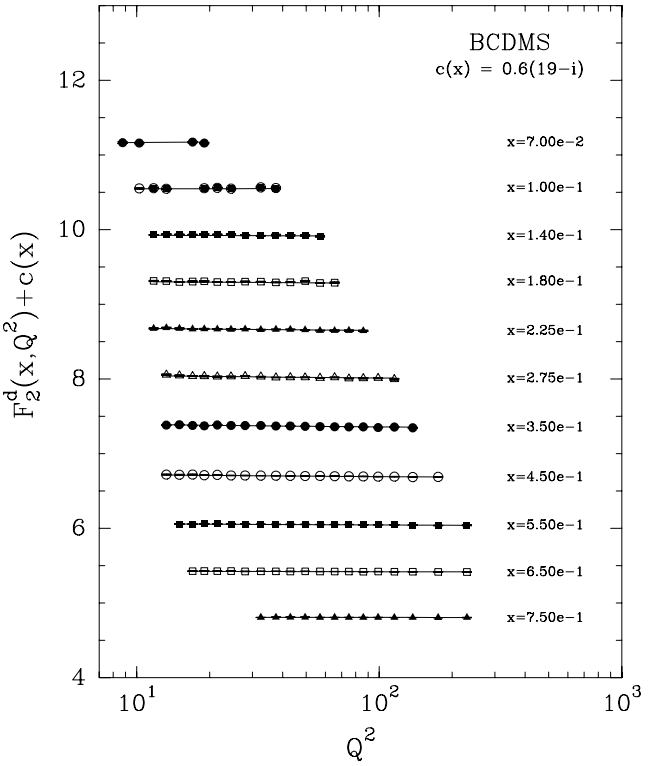

Fig. 13. $F_2^d(x,Q^2)$ as function of Q^2 for fixed x, BCDMS data [21]. The function $c(x_i) = 0.6(19-i)$, $i = 1$ corresponds to $x = 7\ 10^{-2}$.

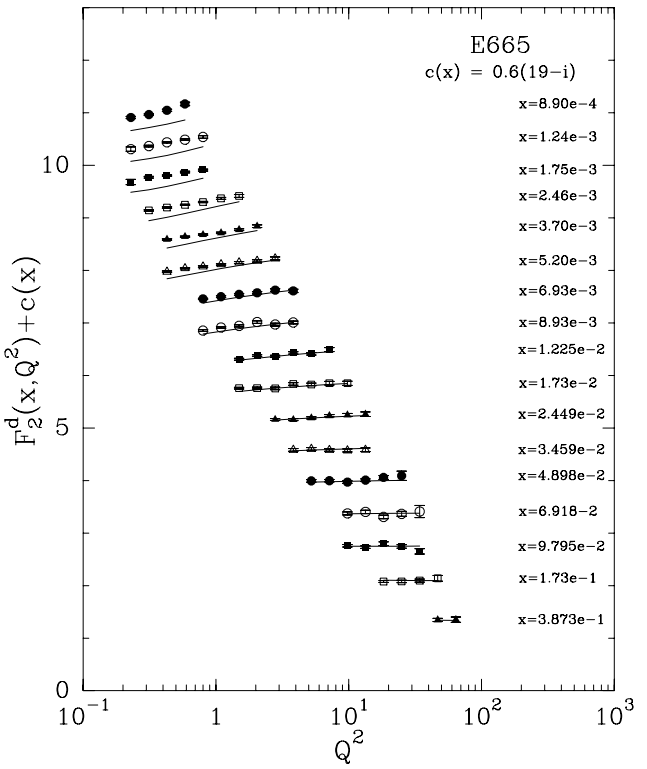

Fig. 14. $F_2^d(x,Q^2)$ as function of Q^2 for fixed x, E665 data [22]. The function $c(x_i) = 0.6(19-i)$, $i = 1$ corresponds to $x = 8.9\ 10^{-4}$.

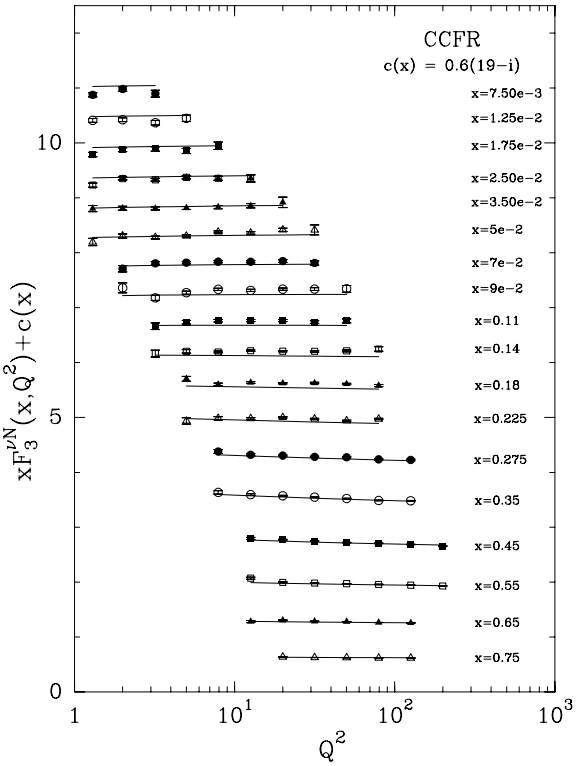

Fig. 15. $xF_3^{\nu N}(x,Q^2)$ as function of Q^2 for fixed x, CCFR data [28]. The function $c(x_i) = 0.6(19-i)$, $i = 1$ corresponds to $x = 7.5\ 10^{-3}$.

$\Delta q_s/q_s = \Delta\bar{u}/\bar{u} = \Delta\bar{d}/\bar{d} = \Delta s/s$. Our model calculations give a very good description of the u and d quark polarizations as shown in the Figure. The comparison between our three curves $\Delta\bar{u}/\bar{u}$, $\Delta\bar{d}/\bar{d}$ and $\Delta s/s$ and the poor accuracy sea quark data does not allow one to draw any conclusion.

In Fig. 20 we show a data compilation of the polarized structure functions $g_1^{p,d,n}(x,Q^2)$ from different current experiments on proton, deuterium and helium targets, evolved at a fixed value $Q^2 = 5\mathrm{GeV}^2$. The x dependence is in fair agreement with our results and we predict, in the small x region, a fast rising behavior for g_1^p and a fast decreasing behavior for g_1^n, due to the antiquark contributions. This cannot be tested so far, due to the lack of precise data. The Q^2 dependence for fixed x values is displayed in Figs. 21 and 22.

Here we would like to comment on the choice we made for $\Delta s(x,Q^2)$ $(\Delta\bar{s})$ in Eq. (17). Clearly this polarized quark distribution is very badly known and we have constrained its first moment by assuming the validity of the second Bjorken sum rule, namely

$$\Delta q_8 = \Delta u + \Delta\bar{u} + \Delta d + \Delta\bar{d} - 2(\Delta s + \Delta\bar{s}) = 3F - D\ , \tag{26}$$

where F and D are the hyperon beta decay constants, so that $3F - D = 0.579$. At $Q^2 = 4\mathrm{GeV}^2$, we have found for the following first moments, $\Delta u = 0.6678$, $\Delta\bar{u} = 0.0464$, $\Delta d = -0.2576$, $\Delta\bar{d} = -0.0865$ and $\Delta s = \Delta\bar{s} = -0.0443$,

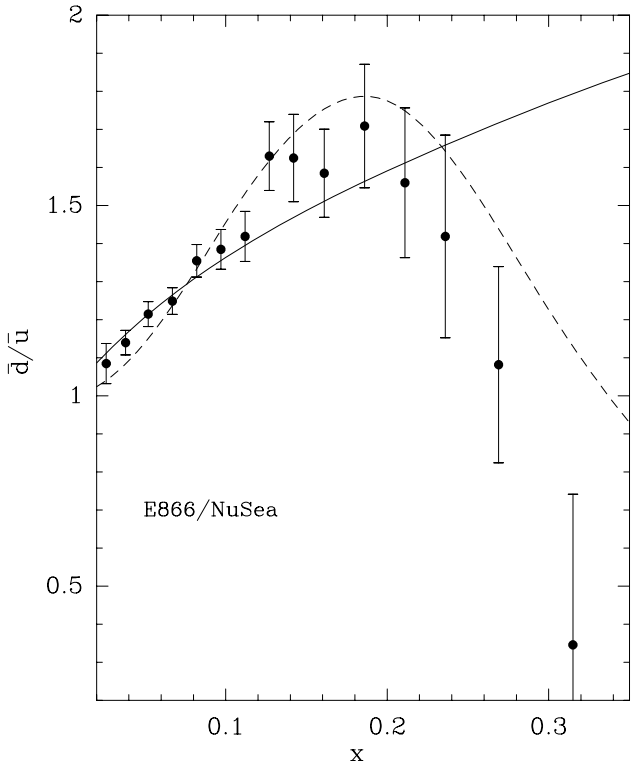

Fig. 16. Comparison of the data on $\bar{d}/\bar{u}(x, Q^2)$ from E866/NuSea at $Q^2 = 54\text{GeV}^2$ [33], with the prediction of the statistical model (solid curve) and the set 1 of the parametrization proposed in Ref. [37] (dashed curve).

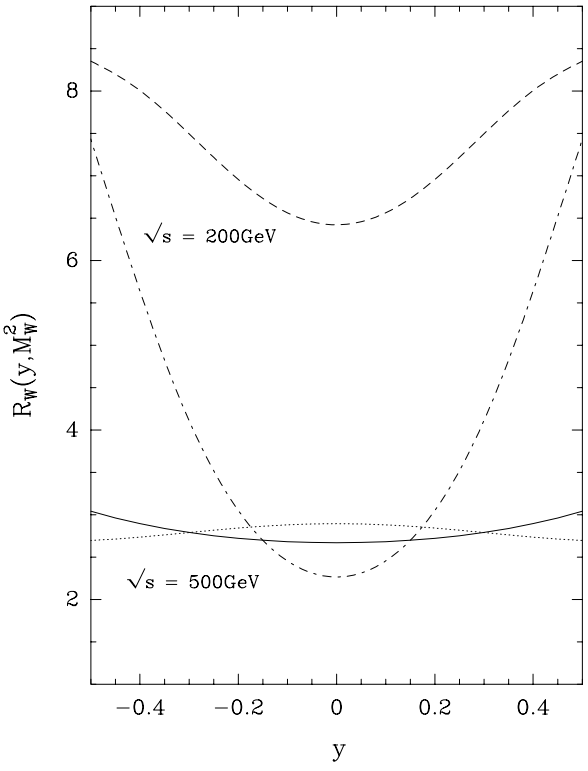

Fig. 17. Theoretical calculations for the ratio $R_W(y, M_W^2)$ versus the W rapidity, at two RHIC-BNL energies. Solid curve ($\sqrt{s} = 500\text{GeV}$) and dashed curve ($\sqrt{s} = 200\text{GeV}$) are the statistical model predictions. Dotted curve ($\sqrt{s} = 500\text{GeV}$) and dashed-dotted curve ($\sqrt{s} = 200\text{GeV}$) are the predictions obtained using the $\bar{d}(x)/\bar{u}(x)$ ratio from Ref. [37].

so $\Delta q_8 = 0.547$. Notice that the first Bjorken sum rule is also very well satisfied, since we get $I_{Bj} = 0.1764$. It is interesting to realize that the contribution of the antiquarks to I_{Bj}, whose value in our case is 0.0221, is positive and relatively large because $\Delta\bar{u}$ and $\Delta\bar{d}$ have the same signs as Δu and Δd, respectively.

Finally we turn to the important issue of the large x behavior of the polarized quark distributions. This kinematic region has been poorly explored experimentally so far, but there are different theoretical scenarios [42], when x is near 1, for the asymmetries $A_1^{p,d,n}(x, Q^2)$, measured in polarized DIS. We recall the definition of the asymmetry $A_1(x, Q^2)$, namely

$$A_1(x, Q^2) = \frac{g_1(x, Q^2)}{F_2(x, Q^2)} \frac{2x[1 + R(x, Q^2)]}{[1 + \gamma^2(x, Q^2)]} , \qquad (27)$$

where $\gamma^2(x, Q^2) = 4M^2x^2/Q^2$ and $R(x, Q^2)$ is the ratio between the longitudinal and transverse photoabsorption cross sections. In the case where the u quark dominates, we get

$$A_1 \sim \frac{\Delta u(x, Q^2)}{u(x, Q^2)} \frac{[1 + R(x, Q^2)]}{[1 + \gamma^2(x, Q^2)]} . \qquad (28)$$

When $x \to 1$ for $Q^2 = 4\text{GeV}^2$, R is of the order of 0.30 or less and $\gamma^2(x, Q^2)$ is close to 1, so $A_1 \sim 0.6\Delta u(x)/u(x)$. It seems unlikely to find $A_1 \to 1$, unless one lets Q^2 go to infinity or one violates positivity. We show in Fig. 23 a compilation of the world data for $A_1^{p,n}(x, Q^2)$ at $Q^2 = 4\text{GeV}^2$, with the results of our calculations up to $x = 1$, where we have $\Delta u/u = 0.77$, $\Delta d/d = -0.46$ and indeed we find $A_1^{p,n} < 1$. This specific prediction should be confronted with the very accurate data on A_1^n in the large x region which is expected soon from Jefferson Lab [43].

5 Helicity asymmetries for weak boson production at RHIC-BNL

Next we propose some tests of our PPD in hadronic collisions in the framework of the spin program at RHIC-BNL [39]. As we have seen in Section 3, the production of $W^{\pm}$ in pp collisions is very relevant to probe the behavior of the $\bar{d}(x)/\bar{u}(x)$ ratio and since W bosons are produced through a pure $V - A$ interaction, they are also an ideal tool to study the spin structure of the nucleon.

Let us consider the parity-violating helicity asymmetry $A_L^{PV}(W)$ defined as

$$A_L^{PV}(W) = \frac{d\sigma_-^W/dy - d\sigma_+^W/dy}{d\sigma_-^W/dy + d\sigma_+^W/dy} , \qquad (29)$$

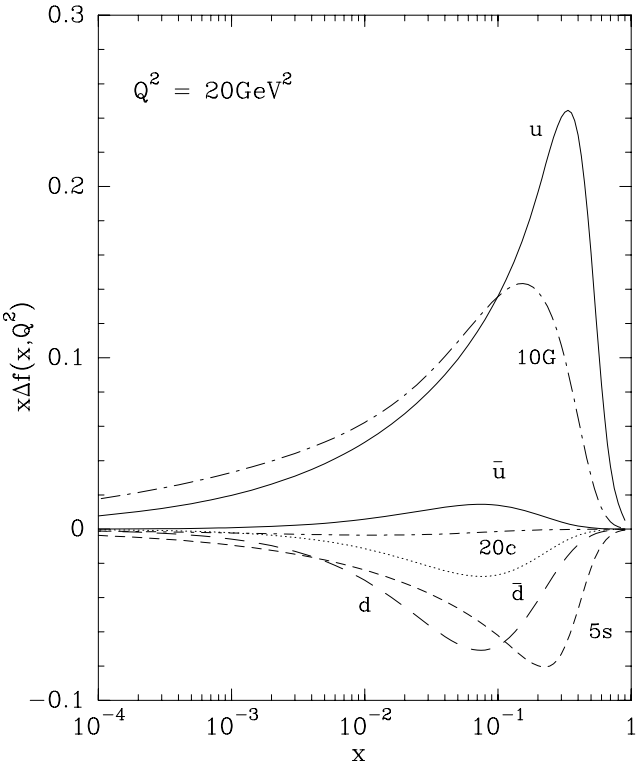

Fig. 18. The different polarized parton distributions (f =u, d, $\bar{u}$, $\bar{d}$, $s(\bar{s})$, c and G) after NLO evolution, at $Q^2 = 20\text{GeV}^2$, as a function of x.

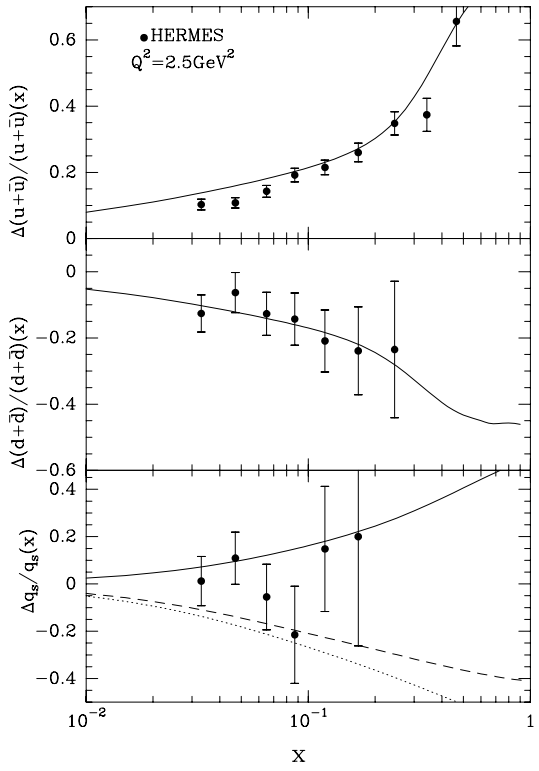

Fig. 19. HERMES data on $(\Delta u+\Delta\bar{u})/(u+\bar{u})$, $(\Delta d+\Delta\bar{d})/(d+\bar{d})$, $\Delta q_s/q_s$ as function of x at fixed $Q^2 = 2.5\text{GeV}^2$ [41]. The curves are our model calculations. For the sea quarks $\Delta\bar{u}/\bar{u}$ (solid curve) , $\Delta\bar{d}/\bar{d}$ (dashed curve) and $\Delta s/s$ (dotted curve).

where $\pm$ stands for the helicity of one polarized proton beam. For W^+, at the lowest order of the Drell-Yan production mechanism, it reads [47]

$$A_L^{PV}(W^+) = \frac{\Delta u(x_a, M_W^2)\bar{d}(x_b, M_W^2) - \Delta\bar{d}(x_a, M_W^2)u(x_b, M_W^2)}{u(x_a, M_W^2)\bar{d}(x_b, M_W^2) + \bar{d}(x_a, M_W^2)u(x_b, M_W^2)}, \quad (30)$$

assuming the proton a is polarized. Here x_a, x_b are defined as in Eq. (25) and for W^- production one interchanges the quark flavor u and d. The calculation of these asymmetries is therefore very simple and the results using our PPD are presented in Fig. 24 at $\sqrt{s} = 350$GeV and 500GeV. The asymmetries decrease for increasing energy and we recall that higher-order corrections have very small effects on these predictions [48]. The general trend of $A_L^{PV}(W)$ can be easily understood and, for example at $\sqrt{s} = 500$GeV near $y = +1$, $A_L^{PV}(W^+) \sim \Delta u/u$ and $A_L^{PV}(W^-) \sim \Delta d/d$, evaluated at $x = 0.435$. Similarly for near $y = -1$, $A_L^{PV}(W^+) \sim -\Delta\bar{d}/\bar{d}$ and $A_L^{PV}(W^-) \sim -\Delta\bar{u}/\bar{u}$, evaluated at $x = 0.059$. Given the expected rates for $W^\pm$ production at RHIC-BNL and the high degree of the proton beam polarization [39], it will be possible to check these predictions of the statistical approach to a high accuracy, in particular for the flavor separation of the antiquarks polarized distributions. [2] It will provide the first reliable determination of $\Delta\bar{u}$ and $\Delta\bar{d}$. One can also consider the asymmetry A_L^{PV} for the Z^0 production whose expression is given in Ref. [47]. Our prediction for this asymmetry is displayed in Fig. 25, but since the Z^0 is not a pure left-handed object the interpretation of the result in terms of the PPD is less obvious than in the $W^\pm$ case. Moreover the Z^0 production rate at RHIC-BNL will be less copious, so the expected precision will be reduced.

In pp collisions for $W^\pm$ production where both protons beams are polarized, there is another observable which is sensitive to the antiquark polarized distributions, that is the parity-conserving double helicity asymmetry $A_{LL}^{PC}(W)$ defined as

$$A_{LL}^{PC}(W) = \frac{d\sigma_{++}^W/dy + d\sigma_{--}^W/dy - d\sigma_{+-}^W/dy - d\sigma_{-+}^W/dy}{d\sigma_{++}^W/dy + d\sigma_{--}^W/dy + d\sigma_{+-}^W/dy + d\sigma_{-+}^W/dy}. \quad (31)$$

For W^+ production it reads, at the lowest order, [38]

$$A_{LL}^{PC}(W^+) = -\frac{\Delta u(x_a, M_W^2)\Delta\bar{d}(x_b, M_W^2) + \Delta\bar{d}(x_a, M_W^2)\Delta u(x_b, M_W^2)}{u(x_a, M_W^2)\bar{d}(x_b, M_W^2) + \bar{d}(x_a, M_W^2)u(x_b, M_W^2)}. \quad (32)$$

[2] For alternative predictions see B. Dressler *et al.*, Eur. Phys. J. C **18**, 719 (2001).

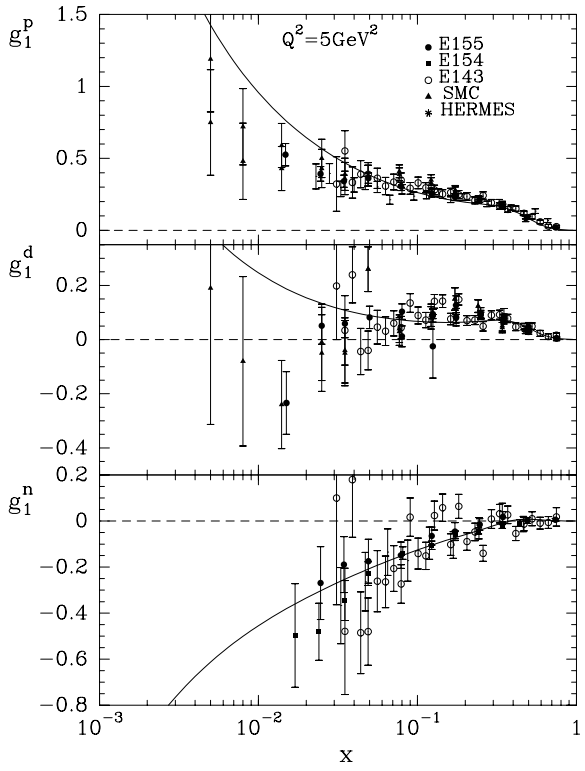

Fig. 20. $g_1^{p,d,n}(x,Q^2)$ as function of x for different Q^2 values, from E155, E154, E143, SMC, HERMES experiments. The curves correspond to our model predictions at $Q^2 = 5\text{GeV}^2$.

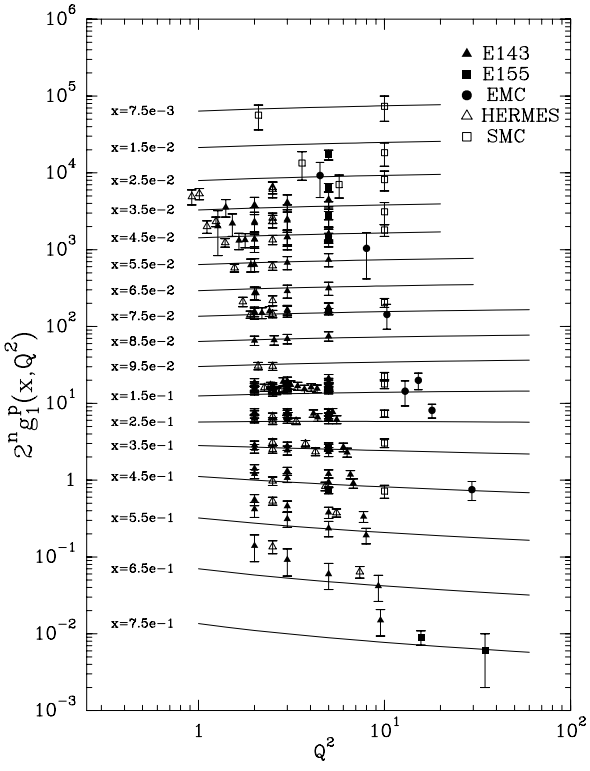

Fig. 21. $2^n g_1^p(x,Q^2)$ as function of Q^2 for different x values. $n = 0$ corresponds to $x = 0.75$ and $n = 16$ to $x = 7.5\ 10^{-3}$. Experimental data are rebined to the nearest x values.

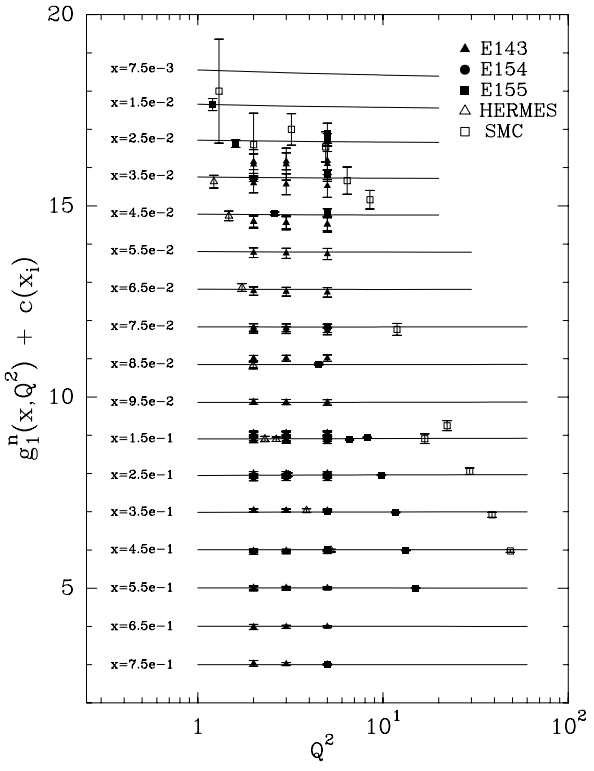

Fig. 22. $g_1^n(x,Q^2)$ as function of Q^2 for different x values. The function $c(x_i) = 19 - i$, $i = 0$ corresponds to $x = 7.5\ 10^{-3}$. Experimental data are rebined to the nearest x values.

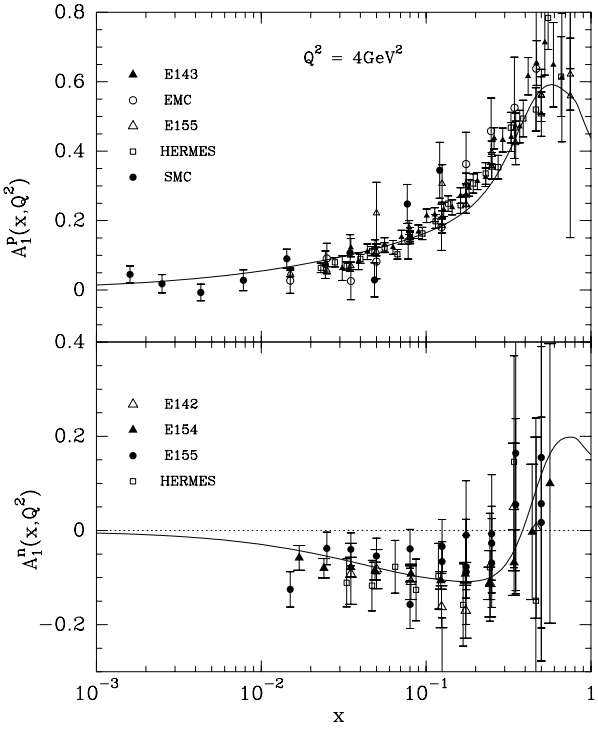

Fig. 23. Compilation of the asymmetries A_1^p and A_1^n from E155, E154, E142, E143, EMC, SMC and HERMES experiments [44]-[46]. The curves correspond to our model predictions at $Q^2 = 4\text{GeV}^2$.

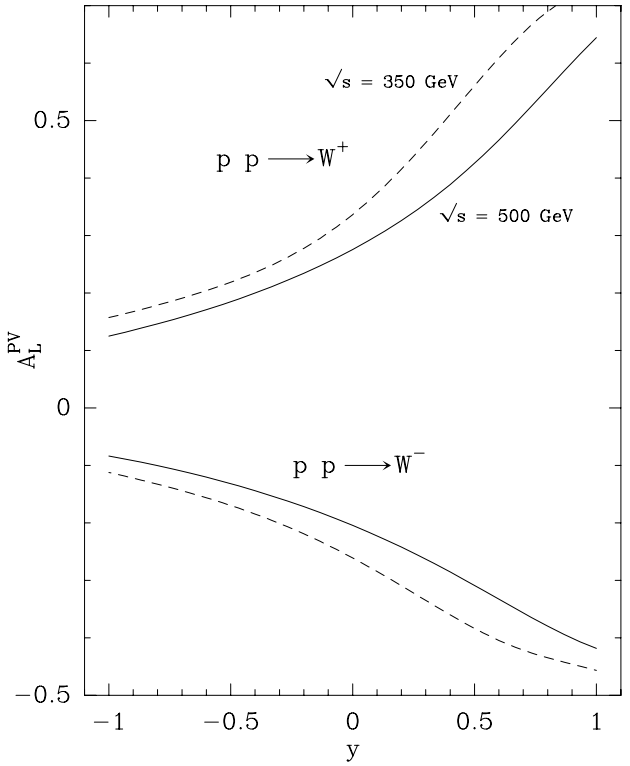

Fig. 24. The parity violating asymmetry A_L^{PV} for $pp \to W^{\pm}$ production versus the W rapidity at $\sqrt{s} = 350$GeV (dashed curve) and $\sqrt{s} = 500$GeV (solid curve).

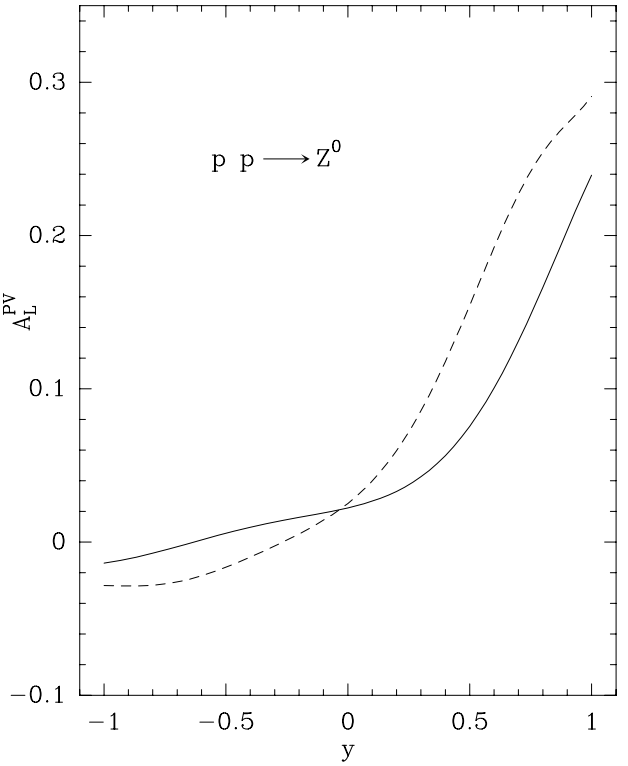

Fig. 25. The parity violating asymmetry A_L^{PV} for $pp \to Z^0$ production versus the Z^0 rapidity at $\sqrt{s} = 350$GeV (dashed curve) and $\sqrt{s} = 500$GeV (solid curve).

We simply notice that if the antiquarks are unpolarized, *i.e.* $\Delta\bar{q}_i(x) = 0$, it leads immediately to $A_{LL}^{PC}(W^+) = 0$. Clearly $A_{LL}^{PC}(W^+)$ is symmetric around $y = 0$ and one obtains $A_{LL}^{PC}(W^-)$ by interchanging the quark flavor u and d. Given the signs of the PPD we have obtained in the statistical approach, it is obvious that $A_{LL}^{PC}(W^{\pm})$ are positive in the y range we are considering, as shown in Fig. 26. The asymmetries decrease for increasing energy but they remain sizeable even at the highest RHIC-BNL energy.

We have also calculated this asymmetry for Z^0 production and the results are presented in Fig. 27. The sign change with respect to $A_{LL}^{PC}(W^{\pm})$ is due to the fact that the expression of $A_{LL}^{PC}(Z^0)$ [38] is driven by terms of the type $-\Delta u(x_a)\Delta\bar{u}(x_b)$ or $-\Delta d(x_a)\Delta\bar{d}(x_b)$, which are both negative in the statistical approach.

Finally let us mention briefly a realistic possibility of having polarized ^3He at RHIC-BNL, which allows to consider pn collisions with polarized neutrons. The same asymmetries can be calculated for this case and, in particular, we have checked that $A_L^{PV}(W^{\pm})$ for $p\overrightarrow{n}$ collisions is directly obtained from $A_L^{PV}(W^{\pm})$ for $p\overrightarrow{p}$ collisions, by exchanging W^+ and W^-, as a consequence of isospin symmetry. For $\overrightarrow{p}n$ collisions with only the proton beam polarized, the results are very close to those obtained for $\overrightarrow{p}p$ collisions.

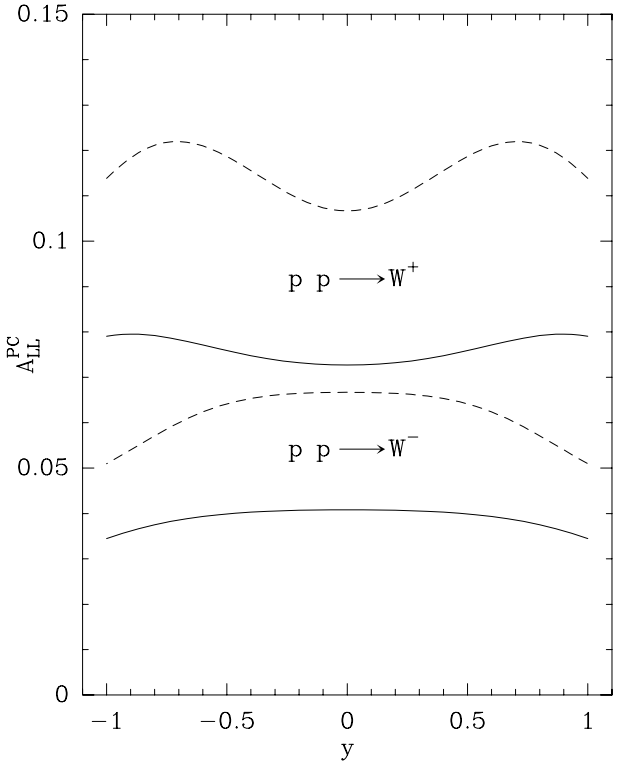

Fig. 26. Parity conserving double helicity asymmetry A_{LL}^{PC} for $pp \to W^{\pm}$ production versus the W rapidity at $\sqrt{s} = 350$GeV (dashed curve) and $\sqrt{s} = 500$GeV (solid curve).

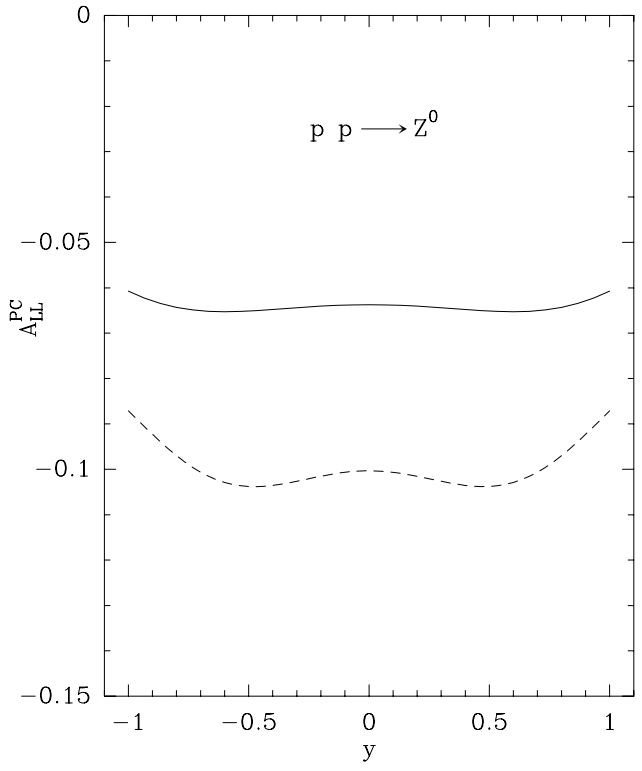

Fig. 27. Parity conserving double helicity asymmetry A_{LL}^{PC} for $pp \to Z^0$ production versus the Z^0 rapidity at $\sqrt{s} = 350$GeV (dashed curve) and $\sqrt{s} = 500$GeV (solid curve).

6 Concluding remarks

We have constructed a new set of polarized parton distributions in the framework of a statistical physical picture of the nucleon. The chiral properties of QCD lead to simple relations between quark and antiquark distributions. We have obtained a good description of all unpolarized and polarized structure functions measured in DIS, $F_2^{p,d}(x,Q^2)$, $xF_3^{\nu N}(x,Q^2)$ and $g_1^{p,d,n}(x,Q^2)$, in a wide kinematic range, in terms of *eight* free parameters, a small number which could be reduced even further. We have also proposed a simple expression for the gluon distribution $G(x,Q_0^2)$, at the input scale Q_0^2, with no additional free parameter. In view of the poor present knowledge of the polarized gluon distribution we took $\Delta G(x,Q_0^2) = 0$. Our analysis of the data was done by using a DGLAP Q^2 evolution at NLO, to get access to a broad kinematic range of x and Q^2. This approach predicts specific flavor symmetry breaking of the light antiquarks. First the inequality $\bar{d}(x,Q^2) > \bar{u}(x,Q^2)$, a natural consequence of the Pauli principle, which is questioned for $x > 0.2$ by the E866 experiment [33]. To answer this challenging issue, we propose to measure the ratio of the unpolarized cross sections for the production of W^+ and W^- in pp collisions at RHIC-BNL, for which we have a definite prediction. Second, this approach leads to $\Delta\bar{u} > 0$ and $\Delta\bar{d} < 0$, so these first moments of the light antiquarks distributions give a positive contribution to the Bjorken sum rule. The precise tests for the x and Q^2 dependence of these distributions will also be done at RHIC-BNL, by the measurements of the helicity asymmetries in the $W^{\pm}$ and Z^0 production, which we have calculated. The strange quarks unpolarized and polarized distributions, are constructed by means of empirical expressions in terms of the light antiquark distributions, but this should be improved in the future with some more fundamental arguments. We have also stressed the relevance of the large x region for the light quark distributions and the behavior of our distributions can be tested in current experiments at Jefferson Lab. Although we still miss a deep understanding of all the features of this approach, as well as a clear interpretation of some of the outgoing parameters, we think it is very promising and challenging in view of the future tests we have identified.

NOTE : We have a much larger comparison of our model predictions with DIS data, by means of many more figures, we could not include in the paper for lack of space. The interested reader can consult the corresponding file accessible at the following address http://www.cpt.univ-mrs.fr/preprints/2001-P.4205/4205-extrafig.pdf .

Acknowledgments: F. Buccella wishes to thank, for warm hospitality, the Centre de Physique Théorique where part of this work was done. We thank T. Gehrmann for providing us his code used in Ref. [48] for NLO Q^2 evolution of the helicity asymmetries. We also thank Z.-E. Meziani, N.Saito, A. W. Thomas and W.Vogelsang for suggestions and fruitful discussions.

References

1. A. Niegawa and K. Sasaki, Prog. Theo. Phys. **54**, 192 (1975); R.D. Field and R.P. Feynman, Phys. Rev. D **15**, 2590 (1977)
2. M. Glück, E. Reya, M. Stratmann and W. Vogelsang, Phys. Rev. D **53**, 4775 (1996)
3. T. Gehrmann and W. J. Stirling Phys. Rev. D **53**, 6100 (1996); R. D. Ball, S. Forte and G. Ridolfi, Nucl. Phys. B **496**, 337 (1997); C. Bourrely, F. Buccella, O. Pisanti, P. Santorelli and J. Soffer, Prog. Theo. Phys. **99**, 1017 (1998); D. de Florian, O. Sampayo and R. Sassot, Phys. Rev. D **57**, 5803 (1998); L. E. Gordon, M. Goshtasbpour and G. P. Ramsey, Phys. Rev. D **58**, 094017 (1998); E. Leader, A. V. Sidorov and D.B. Stamenov, Phys. Rev. D **58**, 114028 (1998); Phys. Lett. B **488**, 283 (2000); Y. Goto *et al.*, Phys. Rev. D **62**, 034017 (2000); M. Botje, Eur. Phys. J. C **14**, 285 (2000); D. K. Ghosh, S. Gupta and D. Indumathi, Phys. Rev. D **62**, 094012 (2000)
4. For a recent review on this very interesting issue see, S. Kumano, Phys. Repts. **303**, 183 (1998)
5. D. de Florian and R. Sassot, Phys. Rev. D **62**, 094025 (2000)
6. M. Glück, E. Reya, M. Stratmann and W. Vogelsang, Phys. Rev. D **63**, 094005 (2001)
7. C. Bourrely, F. Buccella, G. Miele, G. Migliore, J. Soffer and V. Tibullo, Z. Phys. C **62**, 431 (1994)
8. C. Bourrely and J. Soffer, Phys. Rev. D **51**, 2108 (1995)
9. C. Bourrely and J. Soffer, Nucl. Phys. B **445**, 341 (1995)
10. J. Cleymans and R.L. Thews, Z. Phys. C **37**, 315 (1988); E. Mac and E. Ugaz, Z. Phys. C **43, 655** (1989); R.P.

Bickerstaff and J.T. Londergan, Phys. Rev. D **42**, 3621 (1990); J. Cleymans, I. Dadic and J. Joubert, Z. Phys. C **64**, 275 (1994)
11. R.S. Bhalerao, Phys. Lett. B **380**, 1 (1996); R.S. Bhalerao, N.G. Kelkar and B. Ram, Phys. Lett.B **476**, 285 (2000); R.S. Bhalerao, Phys. Rev. C **C63**, 025208 (2001); K. Ganesamurtly, V. Devanathan and M. Rajasekaran, Z. Phys C **52**, 589 (1991); V. Devanathan, S. Karthiyayini and K. Ganesamurtly, Mod. Phys. Lett. A **9**, 3455 (1994); V. Devanathan and J.S. McCarthy, Mod. Phys. Lett. A **11**, 147 (1996); Hai Lin, hep-ph/0105050, hep-ph/0105172, hep-ph/0106100
12. K. Gottfried, Phys. Rev. Lett. **18**, 1154 (1967)
13. New Muon Collaboration, M. Arneodo *et al.* Phys. Rev. D **50**, R1 (1994) and references therein; P. Amaudruz *et al.*, Phys. Rev. Lett. **66**, 2712 (1991); Nucl. Phys. B **371**, 3 (1995)
14. J.D. Bjorken, Phys. Rev. D **1**, 1376 (1970)
15. SLAC E155 Collaboration, P. L. Anthony *et al.*, Phys. Lett. B **493**, 19 (2000)
16. F. Buccella and J.Soffer, Mod. Phys. Lett. A **8**, 225 (1993)
17. F. Buccella, I. Doršner, O. Pisanti, L. Rosa and P. Santorelli, Mod. Phys. Lett. A **13**, 441 (1998)
18. New Muon Collaboration, D. Allasia *et al.*, Phys. Lett. B **258**, 493 (1991)
19. New Muon Collaboration, M. Arneodo *et al.*, Phys. Lett. B **364**, 107 (1995); Nucl. Phys. B **483**, 3 (1997)
20. BCDMS Collaboration, A. C. Benvenuti *et al.*, Phys. Lett. B **223**, 485 (1989)
21. BCDMS Collaboration, A. C. Benvenuti *et al.*, Phys. Lett. B **237**, 592 (1989)
22. FNAL E665 Collaboration, M. R. Adams *et al.*, Phys. Rev. D **54**, 3006 (1996)
23. FNAL E665 Collaboration, M. R. Adams *et al.*, Phys. Rev. Lett. **75**, 1466 (1996)
24. ZEUS Collaboration, M. Derrick *et al.*, Phys. Lett. B **345**, 576 (1995)
25. ZEUS Collaboration, M. Derrick *et al.*, Phys. Lett. B **316**, 412 (1993); Z. Phys. C **65**, 379 (1995); Z. Phys. C **72**, 399 (1996)
26. ZEUS Collaboration, J. Breitweg *et al.*, Eur. Phys. J. C **7**, 609 (1999)
27. ZEUS Collaboration, XXX Int. Conf. High Energy Phys. Osaka (Japan) July 2000, abstract 1049; J. Breitweg *et al.*, Eur. Phys. J. C **11**, 427 (1999)
28. CCFR Collaboration, P. Z. Quintas *et al.*, Phys. Rev. Lett. **71**, 1307 (1993); W. C. Leung *et al.*, Phys. Lett. B **317**, 655 (1993); W. G. Seligman *et al.*, Phys. Rev. Lett. **79**, 1213 (1997); J. H. Kim *et al.*, Phys. Rev. Lett. **81**, 3595 (1998); U. K. Yang *et al.*, Phys. Rev. Lett. **86**, 2741 (2001)
29. SMC Collaboration, B. Adeva *et al.*, Phys. Rev. D **58**, 112001 (1998); Phys. Rev. D **60**, 072004 (1999)
30. SLAC E154 Collaboration, K. Abe *et al.*, Phys. Lett. B **405**, 180 (1997); Phys. Rev. Lett. **79**, 26 (1997)
31. J. Kwiecinski and D. Strozik-Kotloz, Z. Phys. C **48**, 315 (1990)
32. P. Santorelli and E. Scrimieri, Phys. Lett. B **459**, 599 (1999)
33. FNAL Nusea Collaboration, E. A. Hawker *et al.*, Phys. Rev. Lett. **80**, 3715 (1998); J. C. Peng *et al.*, Phys. Rev. D **58**, 092004 (1998); R. S. Towell *et al.*, Phys. Rev. D **64**, 052002 (2001)
34. H1 Collaboration, S. Aid *et al.*, Nucl. Phys. B **470**, 3 (1996); T. Ahmed *et al.*, Nucl. Phys. B **439**, 471 (1995); C. Adloff *et al.*, Nucl. Phys. B **497**, 3 (1996)
35. H1 Collaboration, C. Adloff *et al.*, Eur. Phys. J. C **13**, 609 (2000)
36. H1 Collaboration, S. Aid *et al.*, Nucl. Phys. B **449**, 3 (1995)
37. A. Daleo, C.A. García Canal, G.A. Navarro and R. Sassot, hep-ph/0106156
38. C. Bourrely and J. Soffer, Nucl. Phys. B **423**, 329 (1994)
39. G. Bunce, N. Saito, J. Soffer and W. Vogelsang, Ann. Rev. Nucl. Part. Scie. **50**, 525 (2000)
40. J. Soffer and O. Teryaev, Phys. Lett. B **490**, 106 (2000)
41. HERMES Collaboration, K. Ackerstaff *et al.*, Phys. Lett. B **404**, 383 (1997); Phys. Lett. B **464**, 123 (1999); A. Airapetian *et al.*, Phys. Lett. B **442**, 484 (1998)
42. S.J. Brodsky, M. Burkardt and I. Schmidt, Nucl. Phys. B **441**, 197 (1995); B.-Q. Ma, Phys. Lett. B **375**, 320 (1996); N. Isgur, Phys. Rev. D **59**, 034013 (1999)
43. Experiment E94-110 at TJNAF, Z.-E. Meziani and P. Souder, update to E99-117, Z.-E. Meziani, J. P. Chen and P. Souder
44. EMC Collaboration, J. Ashman *et al.*, Phys. Lett. B **206**, 364 (1988); Nucl. Phys. B **328**, 1 (1989)
45. SLAC E142 Collaboration, P.L. Anthony *et al.*, Phys. Rev. D **54**, 6620 (1996)
46. SLAC E143 Collaboration, K. Abe *et al.*, Phys. Rev. Lett. **75**, 25 (1995); Phys. Rev. D **58**, 112003 (1998)
47. C. Bourrely and J. Soffer, Phys. Lett. B **314**, 132 (1993)
48. B. Kamel, Phys. Rev. D **57**, 6663 (1998); T. Gehrmann, Nucl. Phys. B **534**, 21 (1998)